Insights into microtubule catastrophes: the effect of end-binding proteins and force

Kalisch, S.M.J.

4 How do end-binding proteins affect microtubule dynamics?

A key question in understanding microtubule dynamics is how the microtubule evolves to catastrophe, the transition from assembly to rapid disassembly. Experimental and theoretical efforts provided a range of different mechanisms sometimes supplemented with the results obtained from microtubule regulation by end-binding proteins. To clarify this problem we investigate microtubule dynamics *in vitro* in the absence and presence of end-binding proteins. Using total internal reflection fluorescence microscopy we confirm that the protein complex, consisting of mal3, tea2 and tip1, enhances the MT growth speed and induces catastrophes. We demonstrate that both in the absence and presence of the end-binding proteins catastrophe can be described by a two-step process. Further, we provide evidence that the catastrophe times can be fitted with a gamma and a sequential-step exponential distribution but also with parallel-step exponential distributions. We reason that a catastrophe evolves with a long-timescale step which is followed or accompanied by a shorter step.

4.1 Introduction

For long it has been questioned whether catastrophe is a stochastic process with first order kinetics. This would imply that catastrophe time is independent of the microtubule (MT) age. It would also mean that catastrophe is a one-step process and that events are independent. While some literature regarded catastrophes as randomly distributed and thus first-order events [Hill, 1984, Mitchison and Kirschner, 1987, Dogterom and Leibler, 1993, Flyvbjerg et al., 1994, Howard, 2001, Phillips R., 2008], other literature showed evidence of catastrophe being a multi-step process [Odde et al., 1995, Odde et al., 1996, Stepanova et al., 2010, Gardner et al., 2011b]. These publications provide a range of explanations for catastrophe, the most prominent originating from GTP hydrolysis [Maurer et al., 2012].
As we have shown in chapter 3 MT ends have emerged as dynamic regulatory sites which are bound and modulated by end-binding proteins (EBs). Research has focused on the effect of EB1 (or its homologue mal3), but the observation of other EBs (possibly joint with EB1) might lead to different results.
In order to get a better understanding of the catastrophe process of MTs and

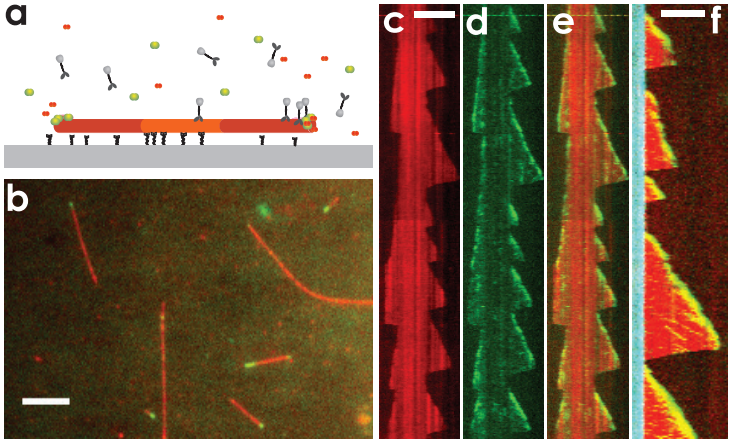

Figure 4.1: Assay of dynamic MTs in the presence of end-binding proteins. a. Schematic setup: dynamic MTs (red) grow from stabilised surface-attached seeds (orange), optionally in the presence of end-binding proteins mal3-alexa488 (green) (and tea2 and tip1 (black/gray)). **b.** TIRF-image of MTs (red) and mal3 (green). **c-e.** Kymographs of the rhodamine-tubulin channel, mal3-alexa488 channel and a colour merge (from left to right). **f.** Kymograph of a (red) MT grown from a blue seed in the presence of unlabelled mal3 and tip1 and green-fluorescent tea2-alexa488. The successful end-tracking proofs the functionality of all three proteins, since tea2 end-tracks only in the presence of both tip1 and mal3 [Bieling et al., 2007]. All scale bar are 5 µm long.

the accompanying role of (individual) end-binding proteins (EBs) we examine dynamic microtubules *in vitro*. The MTs are grown in the presence of tubulin alone, tubulin together with the end-binding protein mal3, or together with mal3, tea2 [Browning et al., 2000, Browning et al., 2003] and the Clip170-homologue, tip1 [Brunner and Nurse, 2000b]. All three proteins are necessary for the correct functioning of tip1 [Bieling et al., 2007]. One function of tip1 has been elucidated in tip1 deletion cells where an increased catastrophe frequency resulted in shortened MTs and misshaped cells [Busch et al., 2004]. In detail the protein complex functions by mal3 associating to the MT lattice with weak affinity but preferentially to the growing MT ends. There it exchanges rapidly and mediates loading of the complex tea2-tip1 which *in vivo* support the transport of growth factors to the growing cell poles. Only when together can tip1 and tea2 move towards and bind to MT's growing plus end where they accumulate [Bieling et al., 2007].

4.2 Results

The stochastic switching of an intact growing microtubule (MT) to a disassembling shrinking MT remains a puzzling subject. With our experiments we want to investigate how a MT transitions to catastrophe. In particular, we want to know whether a

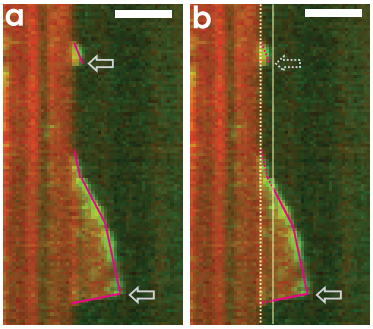

Figure 4.2: Determining MT growth times and MT lengths from kymographs. a. The MT tip was tracked by hand with straight (pink) lines. Each straight line corresponds to growth at constant speed. Transition to shrinkage, termed catastrophe, is indicated with open arrows. Short growth excursions (upper MT) were only counted if they had a signal of 3-by-3 pixels. Longer growth excursions (lower MT) were usually composed of several phases at different constant speeds, here of three growth and one shrinkage phase. Using basic geometry ideas we determined for each line the corresponding growth or shrinkage time (vertical part of the line) and MT length (horizontal part, see text). **b.** The same kymograph as in a. where the seed tip is indicated with a yellow dotted line. When the seed is artificially elongated until its tip ends at the yellow continuous line, all events left of it are discarded (indicated by pink dotted lines and arrow). Only the remaining part of the growth excursions (continuous lines and arrow) are taken for analysis in the same method as described in a. Scale bars represent 3 μm.

catastrophe is a random process or can be better described by a multistep process. Finally we want to gain deeper insight into the nature of the sub-step(s).

4.2.1 Assay to examine microtubule dynamics in the presence of end-binding proteins

In order to address our research questions we grow dynamic MTs from surface-attached stabilised seeds in three conditions. The ambient buffer contained either:
· tubulin
· tubulin and mal3 or
· tubulin and the three EBs, mal3, tea2 and tip1 (referred to as "mal3-tea2-tip1"),
where the latter is shown in figure 4.1a. MTs nucleated from both minus and plus ends of the seed, but for analysis we specifically chose the plus ends. *In vivo* the minus ends are attached to microtubule-organising centres or centrosomes and thus only MT plus ends are relevant in cells. We could differentiate MT plus ends since they assemble faster than minus ends [Allen and Borisy, 1974] and transition more frequently to depolymerisation [Walker et al., 1988].
From the recorded time-lapse TIRF images we created kymographs (space-time plots) for the individual MTs (see fig. 4.1c-e). In these kymographs we tracked the MT ends by hand were we assigned a straight line to a continuous growth or shrinkage phase, for an example see fig. 4.2a. Considering a right-angled triangle where the tracking line is the hypotenuse we could determine MT growth time (vertical side of the triangle) and MT length (horizontal side). From these parameters we could calculate MT growth speed and catastrophe times.
Since only mal3 was fluorescently labelled we could not observe the functionality of tip1 directly. Therefore, we also did experiments with unlabelled mal3 and tip1 and

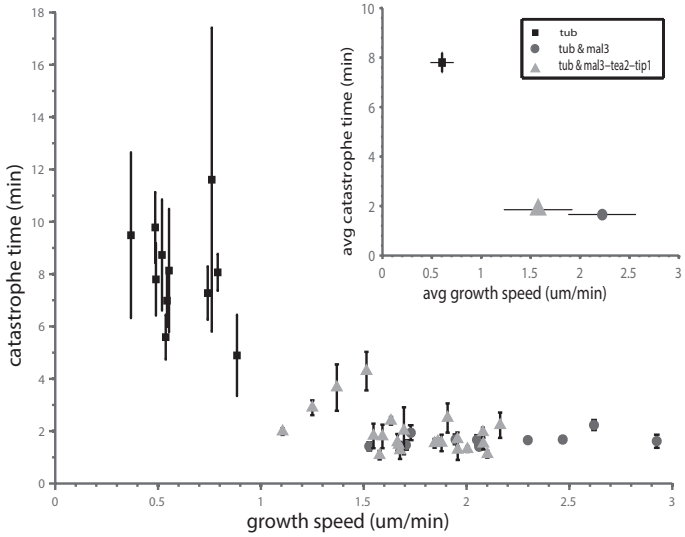

Figure 4.3: End-binding proteins reduce catastrophe time and increase growth speed of free MTs. Each data point represents an average weighted growth speed and catastrophe time per sample. Samples were of three types of conditions: tubulin alone, optionally with the addition of mal3 or of mal3-tea2-tip1. For simplicity we assumed here that catastrophes are random events which allowed us to calculate catastrophe time as the sum of observed growth times per sample over the sum of observed catastrophes. Error of the catastrophe time is $\sqrt{N}$, where N is the number of observed catastrophes per sample. **inset.** To determine the average growth speed per experimental condition we pooled all growth speeds together and weighted each by their growth duration. The error is the weighted standard deviation. The average catastrophe time was calculated as the sum of all observed growth times from the independent samples over the sum of all observed catastrophes. The error is $\sqrt{N_{\text{tot}}}$, where N_{tot} is the total number of catastrophes per experimental condition.

labelled tea2-Alexa488. Under these conditions tea2 end-tracked well (see fig. 4.1f) ensuring the activity of mal3 and tip1 [Bieling et al., 2007].

4.2.2 MTs are more dynamic with EBs

For simplicity we first assumed that catastrophes are randomly distributed, and therefore neither MT growth time ("MT age") nor MT length would influence the catastrophe time. Thus, it did not matter whether a growth event started at the seed or after a rescue and whether it ended with a catastrophe. As a result we determined a catastrophe time per sample τ_c as the sum of all observed growth events in all kymographs of that sample divided by the total number of observed catastrophes. Figure 4.3 shows these catastrophe times τ_c and growth speeds per sample. The different symbols correspond to the three different protein conditions. Compared to the case of pure tubulin, in the presence of the end-binding protein mal3 MTs become more dynamic. Catastrophe times are reduced and growth speeds are

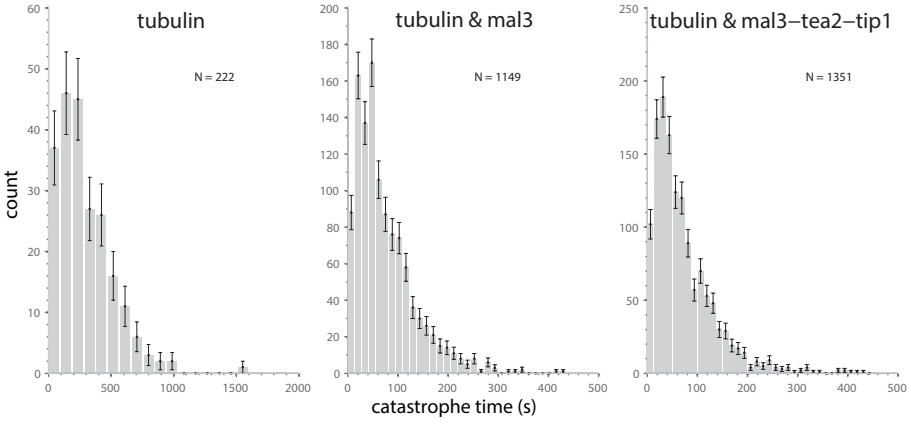

Figure 4.4: Histograms of catastrophes times. N refers to the number of complete growth events from MT nucleation until transition to shrinkage.

increased, agreeing with previous *in vitro* results [Munteanu, 2008, Maurer et al., 2011] (for EB1 [Vitre et al., 2008]). In the presence of mal3, tea2 and tip1 the increase in growth speed and decrease in catastrophe time is almost as strong. The slightly shorter catastrophe time compared to the presence of only mal3 indicates that tip1/tea2 give a slight protection against free catastrophes as shown previously [Munteanu, 2008] and *in vivo* [Brunner and Nurse, 2000b].

4.2.3 Insights into the catastrophe process

As mentioned above, with our work we want to determine whether a catastrophe is a single or multi-step process. Since in the latter case MT age and MT length influences the catastrophe time we now regard only events starting at the seed and ending with a catastrophe. In general, the kinetics underlying a catastrophe can be determined from the catastrophe time distribution. We therefore plot histograms of catastrophe times with objectively determined bin size [Freedman and Diaconis, 1981], see fig. 4.4. Comparing the distributions in the presence of EBs and their absence, the most obvious difference lies in the longer time scale in the tubulin case reflecting the catastrophe-promoting effect of EBs (as mentioned above). To quantify the catastrophe kinetics we fitted the catastrophe times with three different distributions:

- The exponential distribution (fig. 4.5a) is characteristic for first-order transition kinetics and has been assumed to be the prevailing model of catastrophes. In this case an intact MT transitions with rate $k = \tau^{-1}$ to a shortening state.
- The gamma distribution has been used to describe multi-step reactions [Rice, 1995, Floyd et al., 2010, Gardner et al., 2011b]. It represents a non-first order process with several irreversible random steps n where each step happens with an equal characteristic rate k. The probability-density function (pdf) of the gamma

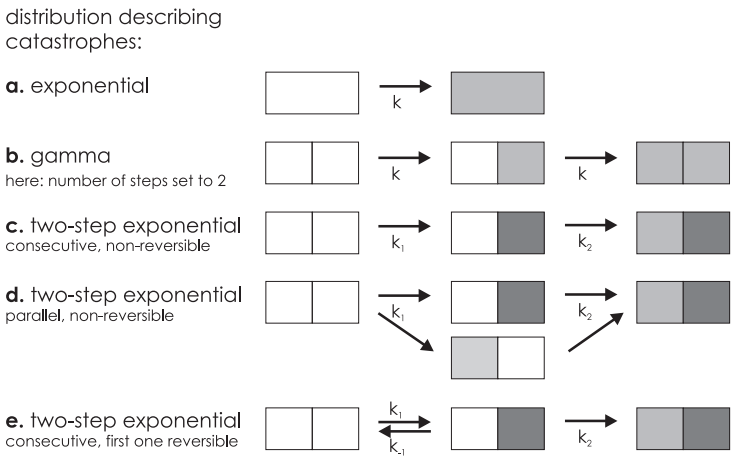

Figure 4.5: Schematic of different catastrophe models. Catastrophes can be described by different models. Here a grey box denotes the accumulation of a catastrophe promoting event. If all boxes are grey the MT transitions to catastrophe. **a.** Catastrophes as stochastic events without memory of the assembly. **b.** Catastrophe happens in several steps where each step is the same and has the same rate. **c.** Two steps are assumed with each a different rate and possibly of different nature. **d.** The two steps can happen in parallel **e.** or one of them can be reversible. The last model was for simplicity not considered for our data. However, we include the special case k_1/k_{-1} which reduces to the distribution described by *a.*

distribution is defined as:

$$\mathrm{f(t)} = \frac{k^n\, t^{n-1}\, e^{-kt}}{\Gamma(n)}, \tag{4.1}$$

where $\Gamma(n)$ is the gamma function. Figure 4.5b shows a gamma process with only two steps, yet in general the gamma distribution represents processes with a number of steps ranging to infinity. (Actually, the exponential is a special case of a gamma distribution with one step.)

- Multiple reactions are also described by a combination of exponentials [Atkins, 1979, Floyd et al., 2010]. Assuming consecutive and non-reversible steps the reaction is described by a "two-step exponential distribution" (fig. 4.5c) [Zhou and Zhuang, 2007]:

$$\mathrm{f(t)} = \frac{k_1 k_2}{k_1 - k_2}(e^{-k_2 t} - e^{-k_1 t}), \tag{4.2}$$

where k_1 and k_2 are the rate constants. This distribution restricts the number of steps to two. On the other hand it allows them to happen with different time scales and thus to be of different nature. Unfortunately, it cannot determine the order of the steps, so k_1 and k_2 are interchangeable.

- If the steps are independent but all necessary to complete the reaction two possibilities emerge:

If the rates k_1 and k_2 are different and in total two steps are allowed we will refer to this distribution as "parallel two-step exponential distribution" (fig. 4.5d). The probability to complete the reaction up to time t is (the cumulative distribution function (cdf)):

$$\mathrm{F(t)} = (1 - e^{-k_1 t})\,(1 - e^{-k_2 t}). \tag{4.3}$$

- If the rates k are the same and the number of steps n is not fixed the probability to complete the reaction up to time t is:

$$\mathrm{F(t)} = (1 - e^{-kt})^n. \tag{4.4}$$

  We call this "parallel multistep-exponential distribution". This function is very similar to the parallel two-step exponential distribution, but, similar to the gamma distribution, it describes processes with same rates and the number of steps as a fit parameter.

In all the above mentioned distributions we assumed the steps towards catastrophe to be irreversible: once a reaction took place it cannot be undone. Generally however, the catastrophe mechanism could comprise a reversible step. Figure 4.5e shows such a reaction where the first step is reversible. In this case the catastrophe process comprises a backward step, meaning the first catastrophe promoting event can be undone. Considering only the first step the combination of forward- and backward-exponential together would yield a peaked distribution. Practically, this would describe a reaction of a fixed time duration. Such a scenario can of course be envisaged as a possible mechanism of catastrophe. However, with our data we would not be able to differentiate such a distribution from a gamma or two-step exponential reaction. Further, with a third parameter we would try to extract more information from our data than is reasonable. Nevertheless, there are two limits which would simplify a distribution with a reversible step. First, if the back-reaction was small, so negligible, we would retrieve the two-step exponential. Second, if on the other hand, the back-reaction was as likely as the forward-reaction, the complete process would be dominated by the second step only. In this case the distribution would be an exponential again. Thus, both cases would not yield more information.

Figure 4.6a shows our data fitted with exponential, gamma and two-step exponential distributions. Obviously in none of the conditions does the exponential distribution fit our data well for short time scales. Those "missing" short-time events indicate that catastrophe is actually a process comprised of several steps. If catastrophe was a first-order process fitting with an exponential distribution would yield the same result as averaging over all (growth) events, as shown in figure 4.3. Clearly, when comparing the two times this is not the case, corroborating that catastrophe is not a one-step process.
The gamma distribution, representing processes with several steps, fits the data better and suggests catastrophe to be comprised of 1.5-1.8 steps (depending on the experimental condition). Since the gamma distribution gives the lower limit on the number of steps [Floyd et al., 2010] and physically only an integer number of steps

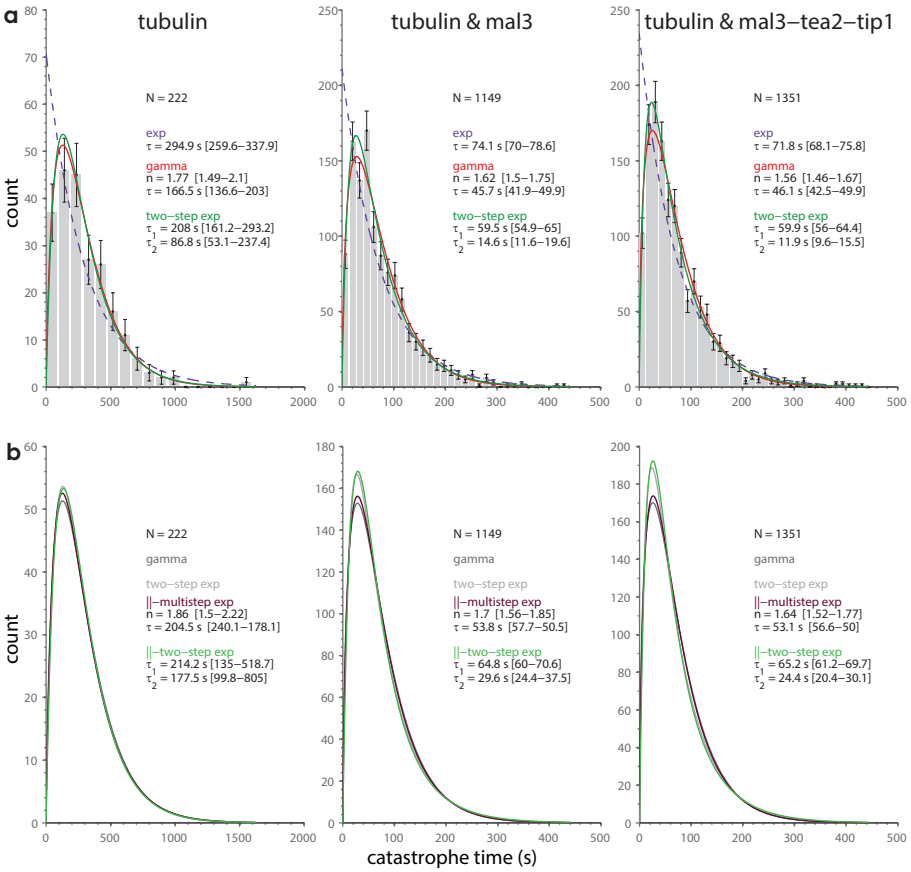

Figure 4.6: Distribution fitting of free catastrophes. Unbinned catastrophe times were fitted with **a.** exponential, gamma and two-sequential step exponential distributions (pdfs) or **b.** with parallel gamma and parallel two-step exponential distributions (pdfs). Histograms of catastrophe times (a.) and the fits are shown where the pdfs are scaled to match the histograms. N refers to the number of complete growth events from MT nucleation until catastrophe. The fit results are displayed in the figure with the 95% confidence intervals in square brackets.

makes sense we identify catastrophe to be a two step mechanism. The fact that our fits gives us an unnatural fraction of a step could be a result of measurement noise. On the other hand, it could indicate that the gamma distribution does not represent our data well. The fraction could be a sign that we do not have two steps of equal time scales and that therefore the imposition of equal rates would be wrong [Floyd et al., 2010].
We therefore also fitted with a sequential-step exponential distribution. Since the gamma distribution fit suggested two steps until catastrophe, we also choose a two-step exponential distribution. Clearly from figure 4.6a these fits are better than the simple exponential distribution for all experimental conditions. They suggest two steps occurring with a shorter and longer rate. As a test, we also fitted with a three-step-exponential distribution. Two of the estimated rates are very similar to the rates from two-step exponential fit, while the third rate is almost zero (data not shown). This is another evidence for the catastrophe mechanism being comprised of two steps.
Also the parallel multistep and parallel two-step exponential distributions fit the data well (fig. 4.6b). The parameter estimates are similar to the fits with the sequential step distributions, except that the time scales are a bit longer. In the parallel two-step exponential case the shorter time even doubled. This makes sense since when the transitions to intermediate states can proceed simultaneously, they can also take longer than if they proceeded sequentially.

4.2.4 The catastrophe mechanism based on information from the long times

It is important to notice that the important information in determining the type of distribution lies in the short time scales. However, these are experimentally hard to determine. Background noise, point-spread function of the microscope and digitisation of the image make it impossible to differentiate MTs shorter than 400 nm from the seed. Even when dynamic MTs and seeds each contain a different fluorophore we do not consider MTs shorter than ~480 nm (in a kymograph this corresponds to a fluorescent intensity of at least 3-by-3 pixels), refer to figure 4.2a. In the presence of EBs shorter events are easier to observe as the mal3 signal is comparably bright. Consequently, differentiation between the absence of a MT and a MT containing a mal3 comet is much easier than in the tubulin case. The lower limit for MTs is hence 320 nm (2-by-2 pixels). Nonetheless, also in this case short events can be faultily detected due to a spread of the signal caused by to the point-spread function of the microscope. Of course, difficulties in detecting the spatial extend of MTs makes it also difficult to define their temporal duration. If it is hard to determine whether a MT nucleated or not makes the exact time of nucleation unclear. In this case a newly nucleated MT can only unambiguously be determined if it has a certain length.
In conclusion, missing short events, more likely in the tubulin case, lower the first bin in the catastrophe time histograms. This results in a less steep rise of the distributions at the short time scales and in a shift towards seemingly more steps

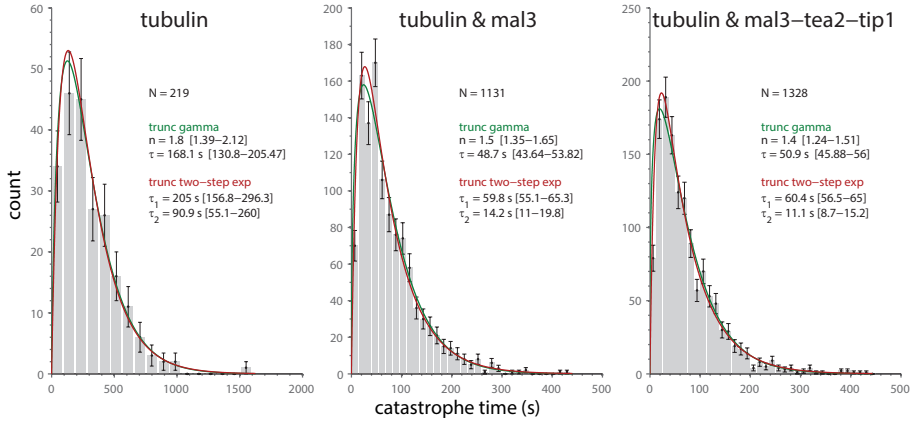

Figure 4.7: Truncated distribution fitting of free catastrophes. Histograms of catastrophe times lasting longer than t_x=10 s, 6 s and 6 s for the case with pure tubulin, with mal3 and with mal3-tea2-tip1, respectively (t_x as an example). The unbinned data was fitted with truncated gamma and truncated two-step exponential distributions (pdfs). N refers to the number of complete growth events from MT nucleation until catastrophe which last longer than the truncation limit. The pdfs are scaled to match the histograms. The fit results are displayed in the figure with the 95% confidence intervals in square brackets.

until catastrophe.

We therefore need a method which takes into account the possible error in determining short-term events. One possible method employs artificially elongating the seed. As illustrated in figure 4.2b we imagine the seed to be a little longer than it is in reality. If a MT nucleates from the real seed and does not grow longer than the "new" seed end, we discard this MT. However, if the MT reaches the new seed end, we consider this as MT "nucleation" and analyse the MT from then on. This "seed-elongation procedure" circumvents the problems we have with determining short events (as explained above) because the artificial short MTs have in reality long, easily observable signals. When plotting the new catastrophe times vs. seed elongation we see that we indeed have a higher number of short events (data not shown). This result is confirmed by fitting with the gamma distribution as the number of steps drops slightly, but does not go to one. Conclusively, this is an indication of an experimental error at the short times. On the other hand, it might obscure or delete a possible effect of MT nucleation from the seed which could influence the MT growth time or MT length of newly nucleated MTs. Besides, by discarding many MTs shorter than the artificial elongation we also "miss" the bias for short MTs. Conclusively, the seed-elongation procedure does not take into account a possible error with the short-time events, and we therefore do not regard it as an appropriate method.

An alternative method using the available information (including the short events)

and its putative error in detecting them will be presented as follows: In our case, catastrophe times are well defined except below a certain threshold t_x. Consequently, we can only reliably fit to the values above t_x. Discarding values below t_x we fit to the remaining data with a so-called left-truncated distribution: it is defined as the original pdf in the limits $[t_x..\infty)$, normalised to integrate to one. A left-truncated distribution is hence defined as [Johnson et al., 1994]:

$$\mathrm{f}_{\mathrm{truncated}}(t, t > t_x) = \frac{\mathrm{f}(t)}{1 - \mathrm{F}(t_x)}, \tag{4.5}$$

where f(t) is the original pdf and $\mathrm{F}(t_x)$ its cumulative distribution function (cdf) at t_x. For an example of fitting with truncated gamma and two-step exponential distributions see figure 4.6.

As we do not have an unambiguous way of fixing t_x in the first place, we varied t_x from 0 to 20 s in half-second steps. We choose this upper limit because we can safely exclude making errors in determining catastrophe times longer than 20 s. Besides, it is a long enough range to see trends in the fit parameters. For each t_x we discarded measured catastrophe times below t_x and fitted the remaining catastrophe times with left-truncated gamma and two-step exponential distributions. The resulting fit parameters are shown in figure 4.8. With the tubulin data we observe little jumps in the resulting fit parameters. They stem from a removal of one or several catastrophe times from the whole distribution. Thus, for t_x<10 s not a single catastrophe time is discarded. The fact that the fit results change nonetheless is a result of the truncation.

In general, we do not detect significant changes in the fit parameters with the tubulin data. When the EBs are present the number of reaction steps goes slightly down, and of course with it, the time scale goes up. This is an evidence that we made an error in determining the short catastrophe times, albeit small. The times determined by the two-step exponential fit change less as the fit is less sensitive to short times.

A truncation t_x from 0 to 20 s is, however, a quite large range and discards at the lower limit too little and at the upper limit of 20 s more data than necessary. To decrease the range we choose a truncation parameter t_x based on a reasonable estimate for the error in determining short events. As mentioned before we could not determine MTs shorter than 3 pixels. With a time-lapse interval of, in average, 3 s with a standard deviation of 1 s we therefore limit the truncation parameter to 6-12 s. The average fit results for this interval can be found in table 4.1.

4.2.5 Simulating gamma and two-step exponential distributions

We proposed four possible mechanisms for catastrophes: multi-step reactions with same rates (gamma and parallel multistep exponenital distribution) and two-step reactions with two different rates ((parallel) two-step exponential distribution). Which of the four distributions explains the data better? A priori we cannot make a differentiation. Consequently, to answer this question and to understand the accuracy of fits to the short time scales we simulated gamma and two-step exponential processes. We choose the parameters such that the distributions looked similar

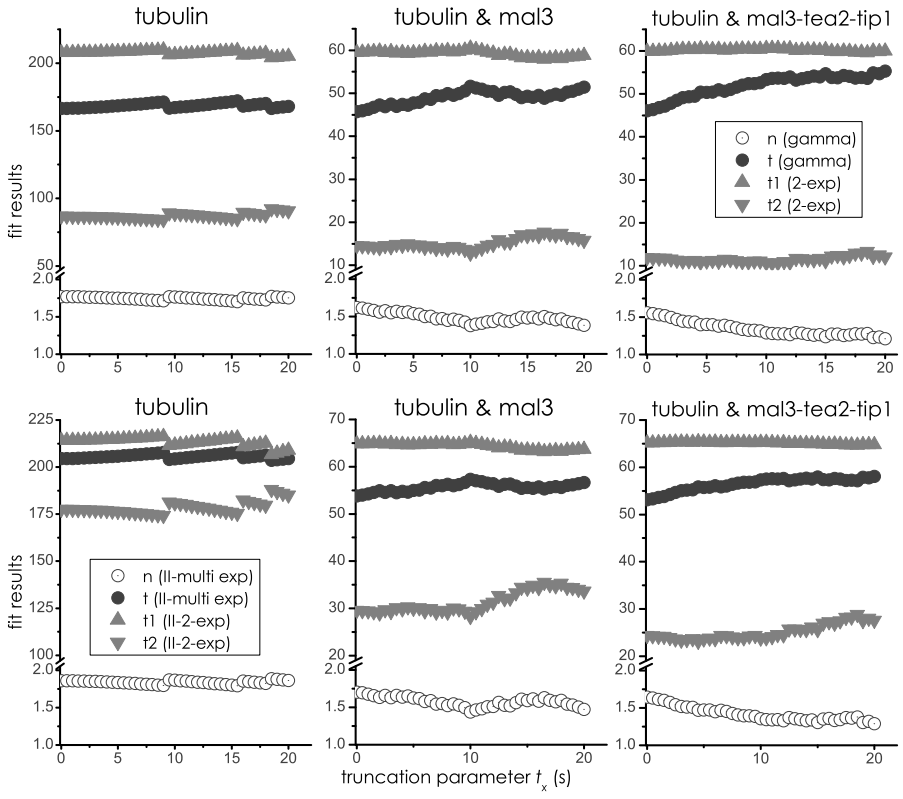

Figure 4.8: Catastrophes of free MTs corrected at short times: fit results. Due to the difficulty and possible error in detecting short events catastrophe times were discarded below a truncation threshold t_x. The remaining data was fitted with **a.** left-truncated gamma and two-step exponential distributions or with **b.** left-truncated parallel gamma and left-truncated parallel two-step distributions. Gamma distributions are more sensitive to the short events. The jumps in the case of pure tubulin happen when one or several complete catastrophe events were discarded. The most reasonable truncation interval is t_x=6 to 12 s corresponding to 3-4 pixels.

to our real data. For that reason we also choose the number of steps to be n=1.5, though a non-integer does not represent a "step". We generated N=200, 1000 or 10^4 random numbers from a gamma distribution and from the sum of two exponentials. After discarding numbers below t_x we fitted the remaining ones with truncated distributions. The truncation parameter t_x was varied between 0 to t_x=20 s in half-second steps (as explained above).
As shown in figure 4.9 with "only" 200 random numbers the truncation fits vary. The reason is that the remaining data after the truncation, so the tail of the distribution is still too noisy to retrieve always the same gamma distribution. With 10^4 numbers statistics improved so that, even after discarding a few numbers, the remaining tail of the distributions is much clearer. As a result, the truncation fits can more reliable find the underlying distribution and fit results vary less. (For better overview we do not show the confidence intervals. As expected, they decrease with improved statistics.) We can conclude that far more than 200 data points are needed to determine the number of steps and the time scales of a reaction reliably. Therefore, and that holds especially for the tubulin data with 222 catastrophe events, the averaging over fits in the truncation range t_x=6 to 12 s improves the reliability of fit results.
Also visible from figure 4.9, the results are influenced by the truncation, especially for N=200. Displaying bigger variations in the fits the gamma pdf is more sensitive to the truncation. Simultaneously it means that the gamma pdf is more sensitive to the crucial short times (especially when the data is generated from two-step exponentials). On the other hand, the two-step exponential cannot easily accommodate changes at the short times which is reflected by the little change of fit parameters during the range of truncations. Therefore we can say that it is less sensitive to the short times. Does the variation in fit parameters mean that the gamma distribution is not the adequate distribution to describe our data? Or does the lack of variation, or in other words, the lack of adaptivity in the two-step exponential case mean that

model	parameter	tubulin	tubulin & mal3	tubulin & mal3-tea2-tip1
gamma	$\bar{n}$	1.74 [1.42-2.06]	1.44 [1.27-1.62]	1.32 [1.17-1.48]
gamma	$\bar{\tau}$	169.1 [133.9-204.2]	50.1 [44.4-55.7]	52.4 [46.7-58.1]
2-exp	$\bar{\tau_1}$	208.2 [161.3-293.7]	59.8 [55.1-65.5]	60.4 [56.4-65.0]
2-exp	$\bar{\tau_2}$	86.6 [52.8-240.8]	14.0 [10.7-20.4]	11.0 [8.4-16.0]
∥-multi exp	$\bar{n}$	1.83 [1.45-2.22]	1.52 [1.31-1.73]	1.39 [1.21-1.58]
∥-multi exp	$\bar{\tau}$	206 [174.4-237.6]	56.3 [51.8-60.8]	56.9 [52.5-61.2]
∥-2-exp	$\bar{\tau_1}$	214.2 [85.8-342.6]	64.8 [59.4-70.2]	65.3 [61-69.5]
∥-2-exp	$\bar{\tau_2}$	177.5 [36.2-318.8]	29.7 [22.8-36.7]	24.1 [18.7-29.6]

Table 4.1: Effect of EBs on the catastrophe process. Catastrophe times were fitted with truncated gamma, truncated two-step exponential (2-exp), truncated parallel multistep exponential (∥-multi exp) and truncated parallel two-step exponential (∥-2-exp) distributions. Mean fit results are shown for truncations between t_x=6-12 pixels with 95% confidence interval in square brackets.

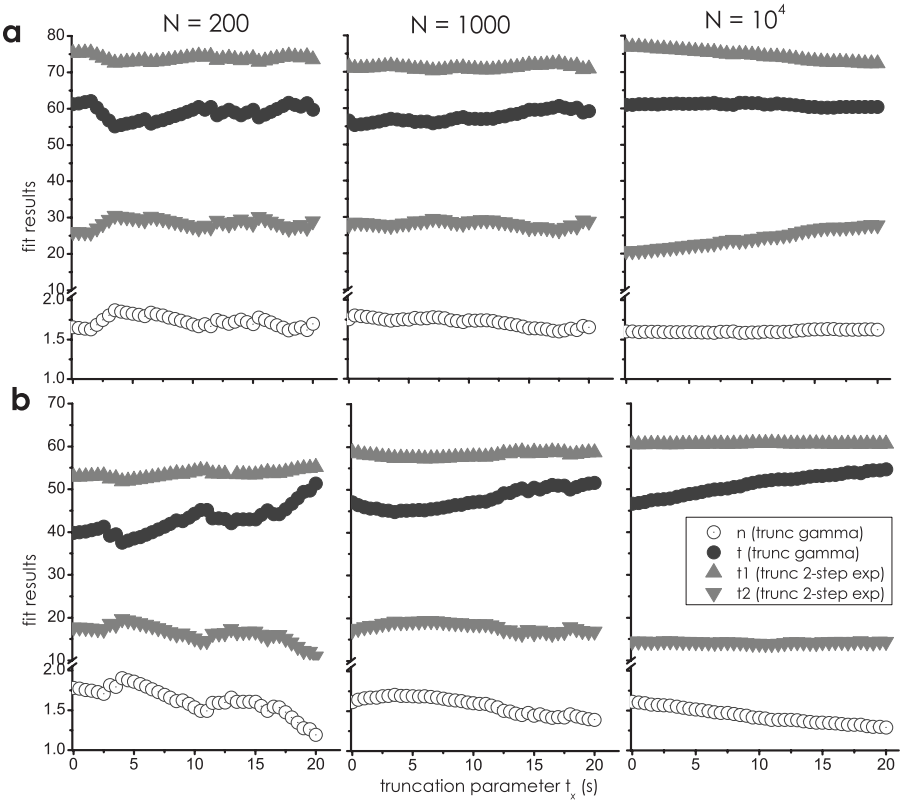

Figure 4.9: Fit results of simulated distributions. N random numbers were generated from **a.** a gamma distribution with n=1.5 and τ=60 s or from **b.** a two-step exponential distribution with τ_1=15 s and τ_2=60 s. Afterwards the unbinned data was fitted with truncated gamma and two-step exponential distributions. Here, the fit results are shown.

it does not represent our data? No matter whether the random numbers are generated from a gamma or two-step exponential distribution we cannot clearly determine which fit is better, even with N=10^4. That means that in our case both gamma and two-step exponential distributions describe the data equally well.
In these simulations we focused only on the sequential-step reactions. However, since fitting with truncated distributions gave similar results for both sequential- and parallel-step reactions we believe to not gain more information by simulations with parallel-step reactions. Consequently, it means that we cannot differentiate whether our data is best described by parallel or sequential-step reactions.

4.3 Discussion

Our data provides insight into the events leading to a transition of MTs from assembly to disassembly. By TIRF microscopy we determined the duration MTs spend in a growing phase. To determine the underlying kinetics we fitted our data with different distributions. Since it is experimentally hard to correctly detect the short events we removed, before fitting, all data below a threshold t_x. Taking this into account, we fitted with probability density functions of truncated distributions whose total probability integrates to one between t_x and infinity. For MTs grown from pure tubulin the truncated gamma distribution suggests n=1.7±0.3 (95% confidence interval (CI)) necessary "steps" until catastrophe. We also fitted with a two-sequential-step exponential which does not constrain the time constants between the steps to be of the same magnitude. It yielded timescales of ~200 s and ~90 s. Further, we allowed the steps until catastrophe to happen simultaneously. With both the parallel gamma and parallel two-step exponential distribution we obtained results similar to those from the sequential-step distributions (except that the shorter timescale of the two-step exponential distribution approximately doubled). Conclusively, we can say that we measure (maximum) two steps until catastrophe. Within our error bars we cannot differentiate whether our data is (parallel) gamma or two-step exponentially distributed.
Gardner et al. [Gardner et al., 2011b] previously measured catastrophe times of green-fluorescent MTs grown from red-fluorescent seeds using TIRF microscopy. This data was fitted with a gamma distribution. Contrary to our results, the authors found catastrophes to happen in two to three steps (depending on the tubulin concentration). Though using lower frame rates (10-20 s) and thus only counting events longer than 45 s they claim that they do not miss the short events. When they shift the fit distribution by 4.5 pixels (a method comparable to our "seed-shift" method) they still do not come close to an exponential function. Considering that their time scale for the completion of one step is in the order of a few hundred seconds, it seems indeed unlikely that the high number of steps is purely a results of missing short events. However, the authors only consider a gamma distribution. We can describe our data also with two-sequential-step exponential or parallel exponential distributions. Similarly, their data might also be represented by a two- or three-step exponential or by a parallel reaction scheme.

What then, tips the tip? If fitting with a gamma distribution is correct, we need two presumably similar processes with the same lifetimes. Gardner et al. [Gardner et al., 2011b] come up with different scenarios: the collection of two protofilaments lacking a GTP cap or the accumulation of structural "defects" like protofilament mismatch or protofilament number. Computational modelling by Margolin et al. [Margolin et al., 2012] showed that the probability for catastrophe is indeed increased if an uncapped protofilament is surrounded by capped long protruding protofilaments. However, it has not been shown that two or three such "gaps" induce the transition to shrinkage. Furthermore, the gamma distribution implies that the MT needs to "remember" the process until a catastrophe. Regarding the "gap" as one event leading to catastrophe it is hard to imagine how such an

uncapped protofilament would not bind a GTP-tubulin until the appearance of the second gap. Likely, changes in protofilament number have been recorded in the MT lattice but it did not seem to be a necessity for catastrophe [Chretien et al., 1992, Chretien et al., 1995].
The two-step exponential model can be realised by two different underlying processes. The MT could accumulate a "defect" which triggers the formation of another "defect" and consequently catastrophe. Those defects could be realised by two different processes, but they could also be of the same nature. Brun et al. [Brun et al., 2009] show in their theoretical paper where a two-step catastrophe after dilution is explained by the hydrolysis of two longitudinally but not laterally adjacent GTPs. In this case each hydrolysis is a sequential step and both steps are of the same nature. However, only after a sudden dilution does this model come up with waiting times in the catastrophe distribution. During growth, the simultaneous hydrolysis and arrival of new subunits produces a narrow peaked, almost exponential distribution and thus cannot explain our data.

To get a better understanding of the catastrophe process it is important to consider also MT catastrophes in the presence of mal3 (and tea2 and tip1). Fitting the EB-data with a gamma or a parallel multistep exponential distribution suggests ~1.4 steps until catastrophe with a catastrophe time of ~50 s. The (parallel) two-step distributions still yield a long and a short lifetime of ~60 s and 10-15 s, while the shorter timescale is approximately doubled with the parallel two-step exponential distribution.
Obviously, the main effect of the EBs is the reduction in catastrophe lifetimes (3-9x). As already mentioned in chapter 3 on page 33 and shown in figure 3.7, Maurer et al. [Maurer et al., 2011, Maurer et al., 2012] suggested EB1/mal3 to be a catastrophe-promoter. Based on their experimental data they concluded that mal3 destroys its own binding site by accelerating the nucleotide transformation of tubulin from an EB1-competent to a GDP-state. The latter state then is not only unfavourable for mal3 attachment but also prone to catastrophe.
The authors [Maurer et al., 2012] also saw that the mal3 intensity, on average, began decreasing linearly about 10 s before the MT switched to depolymerisation and reached the lattice intensity a few seconds after catastrophe. Presumably at this point the EB1-binding region on the MT was depolymerised. As shown in chapter 3 we did the same measurements and came to very similar conclusions. We observed the same decrease of mal3 intensity before the onset of catastrophe lasting in total approximately 20 s. The fact that mal3 disappears before catastrophe renders the EB-binding region a stabilising cap for MTs. Thus, the loss of this region seems to be connected to catastrophes. Since this process occurs only once (disregarding a reset/backward step) it hints at the two steps until catastrophe being of different nature. This makes the (parallel) two-step exponential reaction more likely than the one described by a gamma/multistep distribution. As mentioned, the mal3 intensity-measurements (chapter 3) showed us that the step prior to catastrophe is connected to the transformation of mal3 binding sites and the loss of mal3. We determined this step before catastrophe to be in the order of 20 s which agrees very well to the 15 s we measured for the short-timescale with the two-step exponential

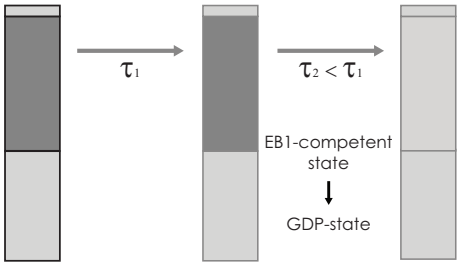

Figure 4.10: The MT transitions to catastrophe. a. An intact MT experiences a catastrophe-promoting event with a relatively long, random time scale. We do not know much about the nature of this event. **b.** The MT, now in an intermediate state, experiences the second catastrophe-promoting event after a random, but shorter time scale. The second event can occur sequential or simultaneous to the first step. It is connected to the nucleotide transition of tubulin from the EB1-competent state into the GDP-state which happens much faster than the step time τ_1. If mal3 was present in the solution it disassociated here from the MT. **c.** After the accomplishment of two random steps the MT undergoes catastrophe and shrinks.

distribution. Also, the parallel two-step exponential comes close. Contrary, it does not agree with the fit results from the gamma/multistep distribution, once more making two processes occurring with the same rate unlikely. We thus envision the transition to catastrophe to occur with a long termed step which is followed or accompanied by a short-timescale step, see figure 4.10. At this moment we do not know much about the nature of the long-term step. During the short-timescale step the tubulin dimers in the MT tip transform from the EB1-competent state into the GDP-state which goes along with the loss of mal3 binding.

Finally, we want to remark on two topics which are though secondary to our research on the catastrophe process. First, it has been shown that *in vivo* a mal3-RNAi leads to shortened MTs indicating it as an essential factor in preventing cytoplasmic catastrophes [Busch and Brunner, 2004]. Our data shows an opposing effect: in the presence of mal3 free catastrophes occurred more often. Here, it is crucial to consider that with a mal3 deletion all associated binding partner loose or alter their function. This leaves the possibility of other factors than the three here-mentioned EBs to modulate catastrophes. Contrary, in our case, we really compare behaviour in the absence and presence of mal3.
Second, as shown in figure 4.3 and published previously [Komarova et al., 2009, Vitre et al., 2008, Katsuki et al., 2009], EBs do not only promote catastrophes but in general, affect dynamic instability parameters. For how they increase the net incorporation of tubulin subunits to the MT end different mechanisms can be imagined: (a) by copolymerisation of tubulin with mal3, (b) recruitment of tubulin to the MT by bound mal3, (c) by promoting the formation of lateral bonds between protofilaments, or (d) by promoting longitudinal bonds between tubulin dimers. Copolymerisation has not been favoured in the literature for two reasons. Gel filtration experiments revealed little interaction between tubulin and mal3 [Bieling

et al., 2007]. Furthermore, individual mal3 molecules turn over rapidly at the MT end while the overall mal3 decoration time at the MT end takes long [Bieling et al., 2007, Maurer et al., 2011]. Together with [Maurer et al., 2012] this is an indicator that mal3 recognises an existing tubulin configuration. Considering that mal3 needs four tubulin dimers to bind, it cannot bind to the terminal dimers [Maurer et al., 2012] making it difficult to envisage the second scenario as well. On the other hand, since longitudinal bonds are formed before lateral ones [VanBuren et al., 2002, Sept et al., 2003] and mal3 needs four tubulins to bind, it might stabilise MTs by stimulating the inter-protofilament connections. Besides, mal3 could direct the dynamic subunit attachment and detachment [Gardner et al., 2011a] to a rapid and stable addition of tubulin and thus faster growth.

4.4 Methods

The experiments described here are based on previous assays as described in section 2.2.2 on page 2.2.1ff.

Sample preparation. Glass cover slips were sonicated for 30 minutes in iso-propanol, then rinsed 3x in MilliQ, sonicated for 20 minutes in 1 M KOH and rinsed 3x with MilliQ. A flow-chamber was assembled by parallelly gluing two strips of parafilm between a microscope slide and a coverslip (Merck, Darmstadt, Germany). The flow chamber was functionalised and passivated with a 0.2 mg/ml mix of biotin-PLL-PEG and PLL-PEG (SurfaceSolutions, Switzerland). Residual non-specific binding sites were blocked with 0.5 mg/ml κ-casein and 1 % F-127. Stabilised, fluorescently labelled MT seeds (containing 12 % fluorescent tubulin and 18 % biotin tubulin) were attached by means of a biotin-streptavidin linker. Microtubule growth was initiated by adding MRB80 buffer (80 mM K-PIPES pH 6.8, 50 mM KCl, 4 mM $MgCl_2$, 1 mM GTP, 1 mM EGTA, 10 mM 2-mercaptoethanol), 0.5 mg/ml κ-casein, an oxygen scavenger system (20 mM glucose, 200 μg/ml glucose-oxidase, 400 ug/ml catalase), 15 μM tubulin of which 5-7 % was labelled with rhodamine, HiLyte488 or HiLyte647 (Cytoskeleton, Denver, CO, USA). Optionally, end-binding proteins (EBs) were added: either 200 nM mal3-Alexa488 alone or together with 8 nM tea2 and 50 nM tip1 (in the latter case also 2 mM ATP was added to the MRB80 buffer). EBs were purified as described in [Bieling et al., 2007]. Unless stated otherwise, chemical reagents were obtained from Sigma-Aldrich (Saint-Louis, MO, USA).

Imaging method. The sample was imaged in an inverted Ti-Nikon Eclipse microscope (Nikon, Tokyo, Japan) using total internal reflection fluorescence (TIRF) microscopy equipped with a 1.49 NA, 100x oil immersion objective. Single tiff-images were recorded using a Calypso 491 nm diode laser (Cobolt, Solna, Sweden), a Jive 561 nm diode laser (Cobolt) and a 635 nm "56 RCS-004" diode laser (Melles Griot, Albuquerque, NM, USA) imaged with a Roper Scientific Coolsnap HQ CCD-camera (Photometrics, Tucson, AZ, USA) and saved to disk with MetaMorph software (Molecular Devices, Sunnyvale, CA, USA), at time-lapse intervals between 0.2 and 5 s, at typical exposure times of 200-250 ms. After mounting the sample on the microscope stage imaging started after a 5 minute equilibration time. Imaging time was kept below 2 hours (average of 1 hour) at a constant temperature of 25 ± 0.5°C which was maintained by running heated/cooled water through a sleeve around the objective. Simultaneously, the water temperature was adjusted by Peltier elements to a

temperature based on a sensor within the sleeve in proximity to the sample.

Data analysis. Tiff-stacks were background-subtracted and bleach-corrected (macro developed by J. Rietdorf, EMBL Heidelberg, Germany) in Fiji (based on ImageJ which was developed by Wayne Rasband, NIH in Bethesda, MD, USA). Growth trajectories of single MTs were displayed in kymographs where straight lines were fitted to each growth or shrinkage phase by hand/mouse. A phase was defined as continuous growth or shrinkage at constant speed. Free growth and shrinkage was differentiated by angle of the line fit. Coordinates of the line fits were processed in Matlab (Mathworks, Natick, NA, USA) by a custom-made software to determine dynamic instability parameters per sample. Average polymerisation speeds were defined as the average over all events weighted with the time span of the individual event:

$$v_{sample} = \frac{\sum v_i t_i}{\sum t_i} \tag{4.6}$$

The error was the weighted standard deviation which reflects the intrinsic variations of dynamic instability [Gildersleeve et al., 1992]:

$$\sigma_{sample} = \sqrt{\frac{n}{n-1} \frac{\sum (v_i - v_{sample})^2 t_i}{\sum t_i}} \tag{4.7}$$

where i denotes an individual event, v_i the speed (growth or shrinkage) of the event i, t_i is the time spanned by the event i, and n stands for the total number of events per sample.
For each sample, between 3-100 MTs were analysed. Samples with identical experimental conditions were grouped into a "dataset". In this case we pooled all speeds together and weighted each with its duration, analogously to equations 4.6 and 4.7.
For section 4.2.2 the catastrophe time was calculated by dividing the total time a microtubule spent in a growing (pausing) phase by the total number of observed catastrophes. The catastrophe rate was the inverse of the catastrophe time.

Fitting. All unbinned data was pooled together for each experimental condition and was used for distribution fitting. The distribution parameters were estimated and the corresponding confidence intervals given by using the maximum likelihood statistics toolbox of Matlab. The exponential distribution was fitted using the *expfit* function, for the gamma distribution we used the *gamfit* function, while all other distributions were fitted with custom functions.

Simulations. Stochastic processes were simulated in Matlab (Mathworks) in two ways. Either random numbers were generated from a gamma distribution with the number of steps n and the time constant τ set to a specific value. Otherwise they were generated from the sum of two exponential distributions with each a fixed time constant τ_1 and τ_2. The total number of events was N=200, 1000 or 10^4.

Acknowledgements

We thank Peter Bieling and Thomas Surrey for help with the protein purification of mal3, tea2 and tip1, Roland Dries for help with the imaging and Magdalena Preciado-Lopez for discussions. The work presented in this chapter was carried out as part of the EU Program AMOCROSS, as part of a "VICI" grant provided by the "Nederlandse Organisatie voor Wetenschappelijk Onderzoek (NWO)" and as

part of the research program of the "Stichting voor Fundamenteel Onderzoek der Materie (FOM)", which is financially supported by the "Nederlandse Organisatie voor Wetenschappelijk Onderzoek (NWO).